Fuel 213 (2018) pp. 207-214

EXPERIMENTAL INVESTIGATION OF THE EFFECT OF ORIFICES INCLINATION ANGLE IN MULTIHOLE DIESEL INJECTOR NOZZLES. PART 1 – HYDRAULIC PERFORMANCE

Salvador, F.J. (*), Lopez, J.J., De la Morena, J., Crialesi-Esposito, M.

CMT-Motores Térmicos. Universitat Politècnica de València, Spain

(*) Corresponding author:

Dr. F. Javier Salvador, fsalvado@mot.upv.es

CMT-Motores Térmicos, Universitat Politècnica de València

Camino de Vera s/n, E-46022 Spain.

Telephone: +34-963879659

FAX: +34-963877659

ABSTRACT

Nozzle hydraulic performance has a significant impact on diesel spray development and combustion characteristics. Thus, it is important to understand the links between the nozzle geometry, the internal flow features and the spray formation. In this paper, a detailed analysis of the impact of the nozzle orifices inclination angle on its hydraulic performance is performed. For this purpose, three different nozzles with included angles of 90, 140 and 155 degrees are evaluated. Instantaneous injection rate and momentum flux are measured on a set of injector operating conditions (mainly injection pressure and discharge pressure). The results show that higher inclination angles lead to smaller mass

flow and momentum flux at steady-state conditions, due to the higher losses at the orifice inlet. These losses are translated in lower both area and velocity coefficients. Nevertheless, the impact of this parameter is limited thanks to the counter-acting effect of the hydrogrinding process, which produces larger rounding radii at the orifice inlet as the included angle increases. Based on the experimental results, correlations of the discharge coefficient as a function of the Reynolds number are obtained and evaluated.

KEYWORDS: diesel nozzle, orifice inclination, flow coefficients, momentum flux

NOMENCLATURE

A	Constant for discharge coefficient vs. Reynolds correlation
A_{180}	Constant for discharge coefficient vs. Reynolds correlation for a theoretical nozzle with 180 degrees included angle
A_0	Constant for discharge coefficient vs. Reynolds correlation for a theoretical nozzle with 0 degrees included angle
A_{eff}	Effective area
A_o	Geometrical area
C_a	Area coefficient
C_d	Discharge coefficient
$C_{d,max}$	Maximum value of discharge coefficient vs. Reynolds
$C_{d,180}$	Maximum value of discharge coefficient vs. Reynolds for a theoretical nozzle with 180 degrees included angle
$C_{d,0}$	Maximum value of discharge coefficient vs. Reynolds for a theoretical nozzle with 0 degrees included angle
C_v	Velocity coefficient
D_o	Geometrical nozzle outlet diameter

$\dot{m}$ Mass flow

$\dot{M}$ Momentum flux

m,n Correlation exponents for the discharge coefficient

P_b Backpressure

P_i Injection pressure

u_{eff} Effective velocity at the orifice outlet

u_{th} Theoretical velocity at the orifice outlet, $u_{th} = \sqrt{\dfrac{2 \cdot (P_i - P_b)}{\rho_f}}$

Greek Symbols

α Nozzle included angle

ΔP Pressure drop, $\Delta P = P_i - P_b$

ρ_f Fuel density

υ_f Fuel kinematic viscosity

1. INTRODUCTION

The fuel injection process is one of the most critical elements in diesel engines to optimize the tradeoff between thermal efficiency and exhaust emissions [1–4]. First, the dynamic behavior of the injection system has a significant impact on aspects such as the injection and combustion duration [5–7] or the combustion noise [8,9]. Additionally, the flow conditions at the injector nozzle outlet affect the spray atomization and fuel-air mixing efficiency [10–14]. Improving atomization and mixing can be particularly important in modern engines, since it can help to increase the usage of Exhaust Gas Recirculation

(EGR) [15,16], necessary to comply with more stringent certification requirements regarding nitrogen oxides (NOx) [17].

In order to optimize the injector nozzle design, it is necessary to understand how each geometrical feature affects the nozzle hydraulics and the spray formation. In this sense, reducing the nozzle outlet diameter has shown to be beneficial to improve atomization efficiency [18,19] and to reduce the maximum liquid length [20–22], avoiding issues related with impingement into the combustion chamber walls [15,23,24]. Nevertheless, negative aspects such as the increase of the total injection and combustion durations (especially at high loads) or the potential appearance of nozzle coking issues [25] may limit the reduction of this parameter. The orifice length (more in particular the length-to-diameter ratio) is also a key parameter, mostly affecting the flow turbulence development [26–28]. Other geometrical factors such as the inlet rounding radii or the conicity can significantly modify cavitation formation inside the nozzle [29–34]. The appearance of this cavitation affects negatively the nozzle permeability [27,35–37], but can help to improve the primary atomization and increase the spray cone angle [38–41]. Salvador et al. [42] pointed out that the shape of the nozzle orifices can also impact the characteristics of the internal nozzle flow. Geometrical aspects of the sac volume and the needle seat area also play a role in the discharge capability of the nozzles [43,44].

Another important aspect of the design of multi-hole injection nozzles is the nozzle included angle. This angle is defined as the cone angle formed by the ensemble of all spray axes. Traditionally, this parameter has been selected based on the spray targeting onto the piston, looking to have a good distribution of the fuel-air mixture between the bowl and the squish regions when the main injection is produced close to Top Dead Center (TDC) [45,46]. Thus, most diesel combustion systems feature included angles in the range of 145-158 degrees. Recently, the development of new combustion modes such as Homogeneous Charge Compression Ignition (HCCI) or Premixed Charge Compression Ignition (PCCI), for which the fuel is injected much earlier into the engine cycle, is driving for the investigation of nozzles with significantly smaller included angles [47]. This results in a significant variation of the inclination angle of the orifice with respect to the injector axis, which can affect the mass flow and momentum at the nozzle outlet according to previous computational studies [48–50]. Nevertheless, there is little experimental work in the literature aiming at understanding the implications of using such nozzles on the nozzle hydraulics and the spray formation.

In the current paper, the hydraulic performance of three multi-hole nozzles with included angles of 90, 140 and 155 degrees has been analyzed. For this purpose, the instantaneous mass flow rate and momentum flux at the nozzles outlet orifices have been measured at different levels of injection pressure. The combination of both measurements has allowed the determination of the characteristic flow coefficients at high needle lift conditions. Statistical correlations for the nozzle discharge coefficient as a function of the Reynolds number and the included angle have been obtained from the experimental results.

The paper is divided in 5 sections. Section 2 describes the nozzles used for the study, as well as the different experimental techniques employed. The injection rate and momentum flux results are analyzed in Section 3. Section 4 analyzes the impact of the included angle on the nozzle discharge coefficient, as well as on the area and velocity coefficients. Finally, the main conclusions of the study are summarized in Section 5.

2. EXPERIMENTAL SETUP

The most significant aspects of the experimental arrangements used along this study are provided in this section. For all the experiments, a standard European diesel fuel has been used. The evolution of the main physical properties of the fuel as a function of pressure and temperature are available in [51].

2.1 Injector nozzles

In this research, a solenoid-driven common-rail fuel injector able to reach up to 200 MPa is used. Three different nozzles have been mounted on this injector. All the nozzles feature the same number of holes (10), nominal outlet diameter (D_o = 0.09 mm), nominal conicity (*k-factor*=1.5) and hydrogrinding level (10%), but differ in terms of their included angle α. In particular, three values of α = 90 (N1), α = 140 (N2) and α = 155 degrees (N3) have been selected. A schematic of the three nozzles used is available in Figure 1.

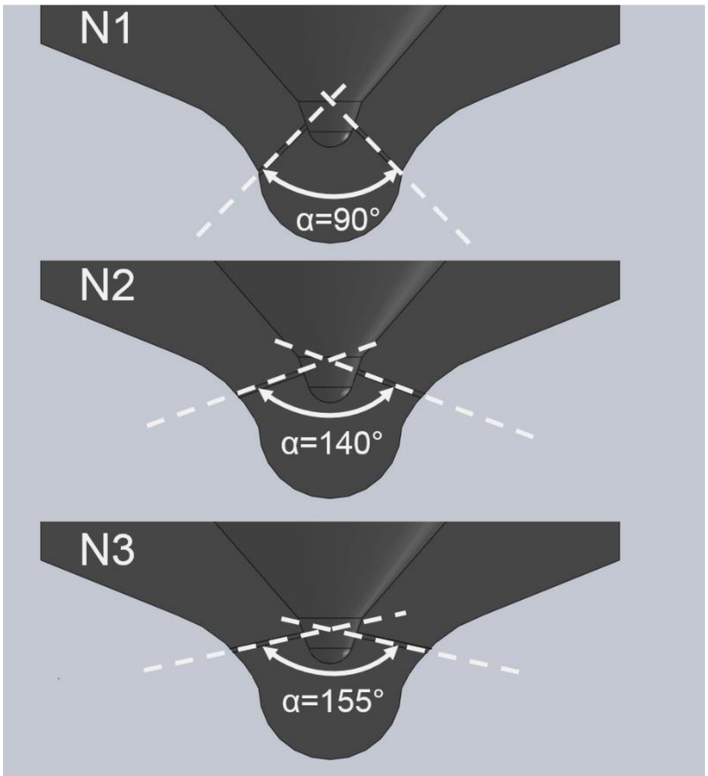

Fig. 1 Schematic of nozzle geometries.

As stated in the introduction, standard included angle values for conventional diesel combustion systems is around 145-158 degrees. This range is properly captured by the selection of nozzles N2 and N3. Recently, new combustion concepts based on LTC modes are proposing lower angles combined with advanced injection timings to achieve more homogeneous mixtures. In this sense, a value a 90 degrees included angle, similar to what it is found in a Gasoline Direct Injection system, can be of interest. Additionally, the range of variation from 90-158 degrees is wide enough to capture the differences in terms of flow direction and hydraulic performance of the nozzle.

2.2 Injection rate meter

An Injection Rate Discharge Curve Indicator system, based on the Bosch method [52], has been used to determine the instantaneous mass flow through the injector nozzle. The measuring device consists on a liquid fuel pressurized tube with a known diameter. The pressure inside the meter is controlled through a pneumatic system using pressurized nitrogen. The fuel injector is mounted on one tip of the tube. When the injector is energized, the fuel delivered by the nozzle generates a pressure increase in the tube, which is proportional to the instantaneous amount of fuel injected. A piezoelectric pressure transducer installed at a few millimeters from the nozzle outlet captures this pressure increase. The pressure signal can be converted into the instantaneous injection rate following the procedure described in [53], with an uncertainty level of ±1.5%. Eight values of injection pressure have been explored, from 23 MPa (minimum injection pressure to achieve a stable injector opening) to 200 MPa (maximum pressure achievable for the solenoid injector used). The backpressure has been maintained constant at 5MPa, which is a typical pressure value for a diesel engine at the start of the main injection. The injector is activated by means of a current signal with a peak value of 20 A, a hold value of 8 A (achieved after 0.4 ms from the start of energizing) and a total energizing time of 1.5 ms.

2.3 Spray momentum test rig

In the case of the spray momentum measurement, the injection is produced in a gas-pressurized chamber at room temperature. The pressure can be set in a range of 0.1-8 MPa, allowing to produce similar density conditions as in a real combustion chamber. During the setup, one of the nozzle orifices is placed perpendicular to the measuring device, consisting on a target coupled to a piezo-electric pressure transducer. When the injection starts and the spray reaches the target, the impact force of the spray is captured. Assuming momentum conservation along the spray axis, the impact force can be considered equal to the momentum flux at the nozzle orifice outlet. The uncertainty of this measurement is approximately ±1.8%. The same test matrix as previously seen for the injection rate measurements has been considered.

The tests were conducted using nitrogen as the filling gas for the spray momentum test rig. For the 90 degrees nozzle (N1), this could lead to a partial overlap of the spray plumes due to the high gas density, affecting the precision of the measurement. In order to assess this potential uncertainty, tests were repeated for this nozzle with helium, which is less dense and produces lower spray opening angles. The results for both gases were almost equal, ensuring that no interaction of different plums was captured by the sensor.

3. EXPERIMENTAL RESULTS

In this section, the main results from the injection rate and momentum flux tests are summarized.

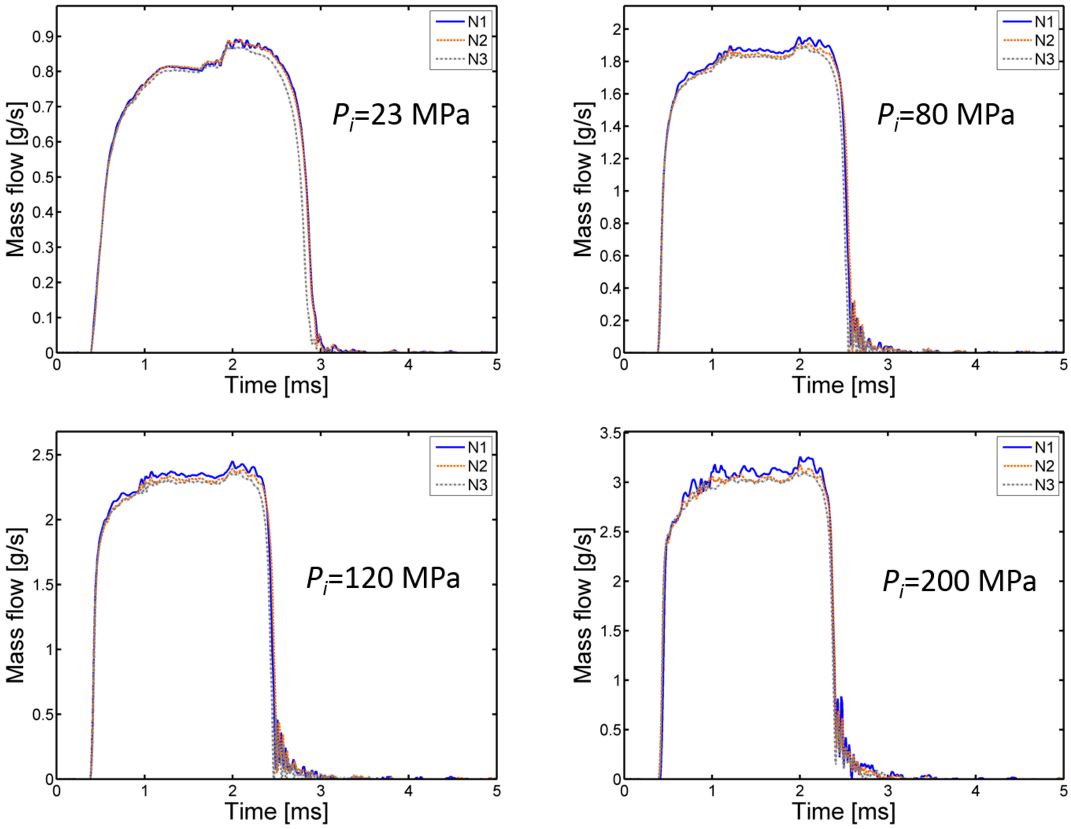

Fig. 2 Mass flow rate results.

In Figure 2, the mass flow rate through a single orifice is provided for the three nozzles previously described and for four levels of injection pressure. Since the fuel injector is the same for all three nozzles, no significant differences can be found during the opening and closing phases of the injection event. This is due to the fact that the instantaneous mass flow rate at low needle lifts is mostly controlled by the needle lift itself, and not so much by the orifice geometry. Once the needle overcomes a certain lift, the flow reaches a nearly steady-state condition and the mass flow depends mostly on the orifice characteristics. There it can be seen how the nozzle with the lowest included angle (N1) produces the highest values of steady-state mass flow, especially as the injection pressure increases. This is related to the lower losses achieved at the orifice entrance, since the flow suffers a lighter change of direction. Regarding the other two nozzles (N2 and N3), the differences found on the mass flow rate are more reduced, but the same trend is still visible.

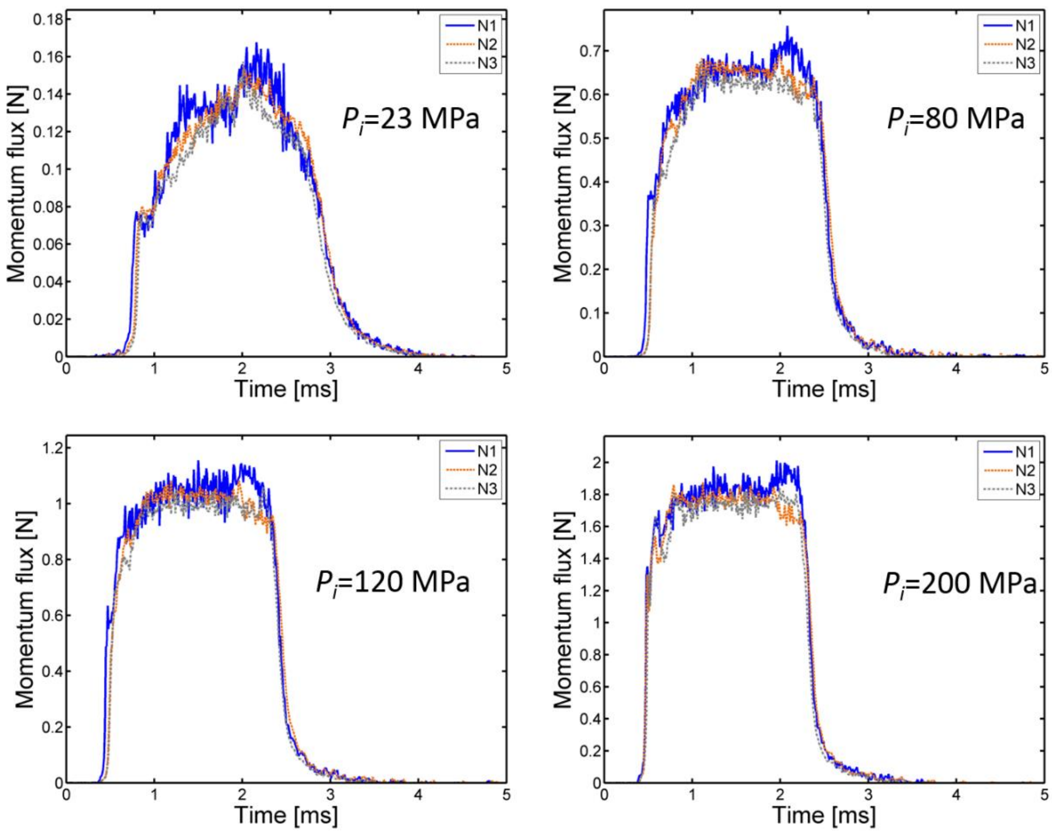

Fig. 3 Spray momentum results.

Figure 3 shows the performance of the three nozzles in terms of spray momentum for the same operating conditions. Although the signals are slightly noisier than in the case of the injection rate, similar conclusions than those already stablished for the mass flow can be drawn. Nevertheless, it is observable that in a relative basis the differences between nozzles N2 and N3 seem to be more pronounced than in the mass flow results, which can be an indicator of the fact that the main effect is related to a decrease in the nozzle outlet velocity. Since the mas flow has a linear dependence on the velocity but the spray momentum depends on the square power of the velocity, the differences can be more significant in the latest. This will anyway be discussed in more detail in Section 4 during the flow coefficients analysis.

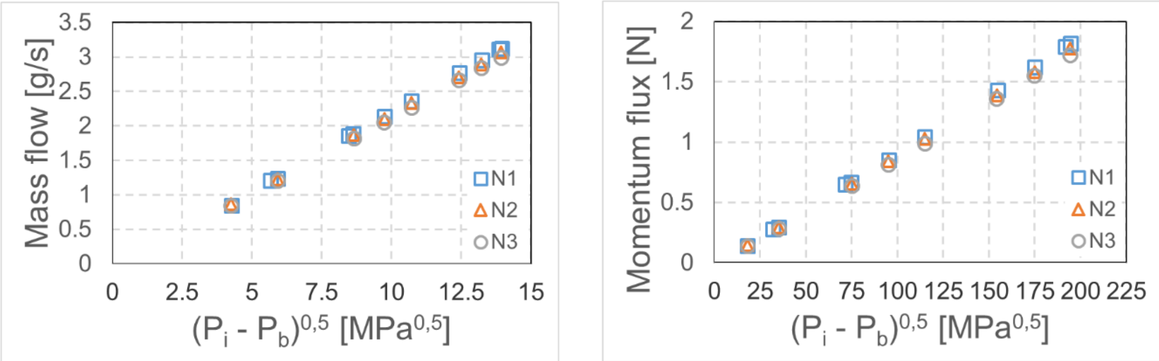

Fig. 4 Steady-state mass flow and momentum flux results.

In Figure 4, the steady-state mass flow and momentum flux delivered by a single orifice of the nozzles are displayed for all the injection pressure cases. These values correspond to a time average of the steady-state phase of the instantaneous mass flow rate and momentum flux curves. The time window to perform this average is manually selected for each injection pressure condition, since this parameter affects the slope of the injector opening ramp and the time lapse between the end of the injector energizing and the start of the needle closing. Once this time window is selected for an injection condition, the same one is applied for both mass flow and momentum flux curves.

In the case of the mass flow, the results are depicted against the square root of the difference between the injection pressure (P_i) and the discharge pressure (P_b). In all cases, it can be observed how the nozzle permeability tends to increase as the nozzle included angle reduces. Nevertheless, the differences among the nozzles is not as significant as it could be expected taking into account the wide included angle variation performed. This could be due to a secondary effect of this angle on the inlet rounding radii produced during the hydrogrinding process, partially compensating the losses at the orifice inlet [48]. It has to be reminded that the hydrogrinding process is performed by flowing an abrasive fluid into the nozzle with 10 MPa injection pressure and 0.1 MPa backpressure. When the included angle is high, the curvature of the flow when entering the orifice is also very intense, producing a higher erosion of the upper-inlet corner of the orifice (i.e., higher inlet rounding radii). This tends to increase significantly the nozzle permeability, since most of the pressure losses are generated in this region, especially as injection pressure ramps up. When the included angle is low, the erosion from this abrasive fluid is more uniformly distributed in the complete geometry of the nozzle, so the inlet rounding radii effect is reduced.

4. HYDRAULIC COEFFICIENTS

The previously discussed results of steady-state mass flow can be also expressed in terms of the nozzle discharge coefficient, which can be defined as the ratio between the actual mass flow and the theoretical one, calculated using the geometrical orifice outlet area A_o and the theoretical velocity u_{th} obtained from Bernoulli's formulation:

$$C_d = \frac{\dot{m}}{\rho_f A_o u_{th}} = \frac{\dot{m}}{A_o\sqrt{2\Delta P \rho_f}} \tag{1}$$

where ρ_f is the liquid fuel density and $\Delta P = P_i - P_b$.

The discharge coefficient values obtained from equation (1) for the three nozzles are depicted in Figure 5 against the theoretical Reynolds number, which is defined as:

$$Re = \frac{u_{th} D_o}{\nu_f} \tag{2}$$

where D_o is the geometrical orifice outlet diameter and ν_f is the fuel kinematic viscosity.

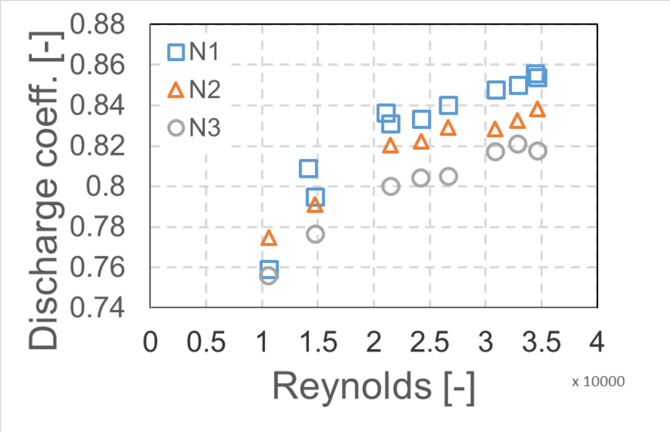

Fig. 5 Discharge coefficient vs. Reynolds number.

Figure 5 shows how the discharge coefficient tends to grow when increasing the Reynolds number. This is due to the development of the boundary layer created around the orifice walls. Previous works in the literature [54,55] show that this behavior can be reproduced by the following equation:

$$C_d = C_{d,max} - \frac{A}{\sqrt{Re}} \qquad (3)$$

where $C_{d,max}$ and A are constants that depend mostly on the nozzle geometrical characteristics. According to this equation, as the Reynolds number increases, the turbulence flow reaches a fully-developed state and the discharge coefficient reaches its asymptotic value.

Equation (3) has been used to obtain statistical correlations for the discharge coefficient as a function of the Reynolds number for the three nozzle geometries used along the study. Table 1 summarizes the results obtained from this statistical analysis. As it can be seen from the high R-squared values achieved, all the correlations show a significant capability to reproduce the experimental data. Additionally, it is appreciable how increasing the included angle produces not only a decrease on the maximum discharge coefficient, but also a decrease on its sensitivity to the Reynolds number (this last statement can be demonstrated because the parameter *A* decreases in a much higher extent than the parameter $C_{d,max}$). This occurs because higher inclination angles induce higher losses at the orifice entrance, so the relative importance of the boundary layer characteristics on the discharge coefficient diminishes [48].

Table 1. Summary of statistical correlations for the discharge coefficient for each nozzle.

Nozzle	$\boldsymbol{C_{d,max}}$	***A***	**R-squared [%]**
N1	0.950	16.99	98.68
N2	0.922	15.49	98.81
N3	0.911	14.85	99.46

Based on the previous results, a new correlation for the discharge coefficient is proposed, where the values of $C_{d,max}$ and *A* are calculated as a function of the included angle α as follows:

$$C_{d,max} = C_{d,180} + \left(C_{d,0} - C_{d,180}\right) \cdot exp\left(-m\frac{180-\alpha}{180}\right) \tag{4}$$

$$A = A_{180} + (A_0 - A_{180}) \cdot exp\left(-n\frac{180-\alpha}{180}\right) \tag{5}$$

In these equations, Cd,180 and A180 represent the values of Cd,max and A that would be obtained for a theoretical nozzle with 180 degrees included angle, while the values of Cd,180 and A180 represent the same magnitudes for a theoretical nozzle with 0 degrees included angle.

Table 2. Summary of statistical correlation for the discharge coefficient

Parameter	***Value***	***Interval of Confidence***
$C_{d,180}$	0.858	[0.81,0.91]
$C_{d,0}$	0.955	[0.94,0.97]
A_{180}	18.31	[16.44,20.18]
A_0	10.37	[5.43,15.32]
m	5.38	[1.7,9.1]
n	5.15	[1.5,8.8]
R-squared	**98.99%**	

The results of this new correlation are summarized in Table 2 and Figure 6, which represents the experimental values against the prediction obtained from the correlation. Again, the high R-squared value confirms the suitability of the formulation proposed to reproduce the experimental trends achieved. Additionally, all of the coefficients show a statistical significance on the C_d correlation, which reinforces the fact that the inclination angle affects both the asymptotic and Reynolds-dependent terms.

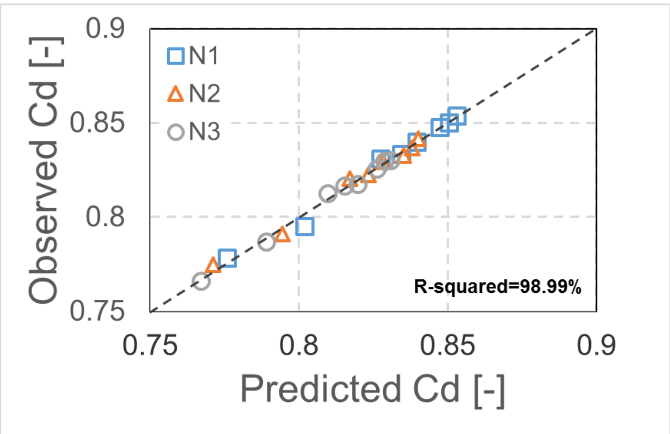

Fig. 6 Observed vs. predicted discharge coefficient.

Finally, Figure 7 shows the comparison between the experimental and predicted values in a discharge coefficient vs. Reynolds evolution. It can be seen that the trends of the experimental results is properly captured by the correlation.

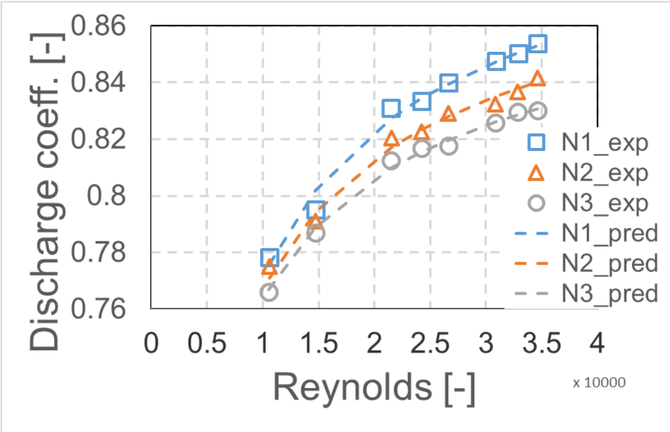

Fig. 7 Experimental and predicted discharge coefficient vs. Reynolds.

The steady-state mass flow and momentum flux can be also expressed as a function of the effective outlet area (A_{eff}) and the effective outlet velocity (u_{eff}):

$$\dot{m} = \rho_f A_{eff} u_{eff} \tag{6}$$

$$\dot{M} = \rho_f A_{eff} u_{eff}^2 \tag{7}$$

Thus, from the combination of both experimental values, it is possible to determine the effective outlet velocity as the ratio between the spray momentum and the mass flow. Once u_{eff} is known, other two non-dimensional flow coefficients can be defined [26]:

$$C_v = \frac{u_{eff}}{u_{th}} = \frac{u_{eff}}{\sqrt{\frac{2\Delta P}{\rho_f}}} \tag{8}$$

$$C_a = \frac{A_{eff}}{A_o} = \frac{C_d}{C_v} \tag{9}$$

where C_v is the velocity coefficient and C_a is the area coefficient. Figure 8 highlights the evolution of these two coefficients against the Reynolds number. As it can be seen, the velocity coefficient shows a very similar evolution with respect to the one already seen for the discharge coefficient. Regarding the area coefficient, the values are roughly constant except for very low injection pressure levels (P_i=23 and 40 MPa). Additionally, the values are close to the unity, meaning that no significant cavitation appears inside the nozzles tested [32]. Even though the differences are small, it is still appreciable how the nozzle with the lowest included angle (N1, 90º) reaches slightly higher C_a values, probably as an indication of the fact that the outlet velocity profile is more symmetric since it is less affected by the recirculation zone generated in the orifice entrance.

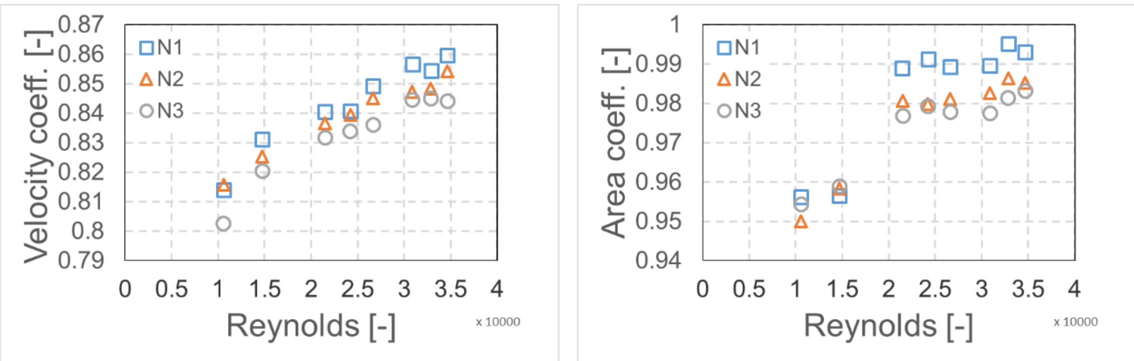

Fig. 8 Area and velocity coefficients vs. Reynolds number.

5. CONCLUSIONS

In the current paper, an investigation of the effect of the orifices inclination angle on the nozzle hydraulics was performed. For this purpose, three multi-hole nozzles with included angles of 90, 140 and 155 degrees were evaluated. The nozzle hydraulic performance was assessed from the measurements of the instantaneous mass flow rate and momentum flux at the nozzle outlet. A significantly wide range of injection pressures (23-200 MPa) was considered.

The opening and closing phases of the injection rate profile showed almost no dependence on the inclination angle, as they were mostly affected by the needle lift profile. Nevertheless, the mass flow achieved on the steady-state phase of the injection event was lower as the inclination angle increases. This was due to the higher losses produced at the orifice entrance, linked to the strongest change in the flow direction. Nevertheless, the differences are lower than what could be expected from the wide variation of the inclination angle explored. This was probably due to the effect that this angle had on the hydrogrinding process performed during the nozzles manufacturing, resulting in larger inlet rounding radii as the orifice inclination increased, partially compensating the effect of the angle itself. Similar conclusions were obtained from the momentum flux results.

The nozzle discharge coefficient was evaluated from the time-average mass flow obtained during the steady-state phase of the injection rate. It was observed how the discharge coefficient grew when increasing the Reynolds number, as a consequence of the higher flow development. Statistical correlations of C_d vs. Re were obtained based on previous experiences from the literature. The analysis of these correlations showed that the inclination angle of the orifices influences not only the maximum discharge coefficient value, but also the slope of its evolution with respect to the Reynolds number.

Finally, the combination of the steady-state mass flow and momentum flux results allowed to determine the nozzle area and velocity coefficients. The area coefficient showed to be mostly independent on the Reynolds number and close to the unity, except at very low injection pressure ($P_i \leq 40$ MPa). The effect of the inclination angle on the area coefficient was reduced, although slightly higher values were achieved for the nozzle with the lowest angle. Regarding the velocity coefficient, similar evolution as the one already indicated form the discharge coefficient was obtained.

ACKNOWLEDGEMENTS.

This work was partly sponsored by "*Ministerio de Economía y Competitividad*", of the Spanish Government, in the frame of the Project "*Estudio de la interacción chorro-pared en condiciones realistas de motor*", Reference *TRA2015-67679-c2-1-R*.

References

[1] Mohan B, Yang W, Chou SK. Fuel injection strategies for performance improvement and emissions reduction in compression ignition engines—A review. Renew Sustain Energy Rev 2013;28:664–76. doi:10.1016/j.rser.2013.08.051.

[2] Suh HK, Lee CS. A review on atomization and exhaust emissions of a biodiesel-fueled compression ignition engine. Renew Sustain Energy Rev 2016;58:1601–20. doi:10.1016/j.rser.2015.12.329.

[3] Gill DW, Ofner H, Stoewe C, Wieser K, Winklhofer E, Kato M, et al. An Investigation into the Effect of Fuel Injection System Improvements on the Injection and Combustion of DiMethyl Ether in a Diesel Cycle Engine. SAE

Tech Pap 2014-01-2658 2014. doi:10.4271/2014-01-2658.Copyright.

[4] Kim D, Martz J, Violi A. Effects of fuel physical properties on direct injection spray and ignition behavior. Fuel 2016;180:481–96. doi:10.1016/j.fuel.2016.03.085.

[5] Ferrari A, Mittica A. Response of different injector typologies to dwell time variations and a hydraulic analysis of closely-coupled and continuous rate shaping injection schedules. Appl Energy 2016;169:899–911. doi:10.1016/j.apenergy.2016.01.120.

[6] Salvador FJ, Gimeno J, De la Morena J, Carreres M. Using one-dimensional modeling to analyze the influence of the use of biodiesels on the dynamic behavior of solenoid-operated injectors in common rail systems: Results of the simulations and discussion. Energy Convers Manag 2012;54:122–32. doi:10.1016/j.enconman.2011.10.007.

[7] Payri R, Salvador FJ, Gimeno J, De la Morena J. Influence of injector technology on injection and combustion development, Part 2: Combustion analysis. Appl Energy 2011;88:1130–9. doi:10.1016/j.apenergy.2010.10.012.

[8] Patel C, Lee S, Tiwari N, Agarwal AK, Lee CS, Park S. Spray characterization, combustion, noise and vibrations investigations of Jatropha biodiesel fuelled genset engine. Fuel 2016;185:410–20. doi:10.1016/j.fuel.2016.08.003.

[9] Zhuang J, Qiao X, Bai J, Hu Z. Effect of injection-strategy on combustion, performance and emission characteristics in a DI-diesel engine fueled with diesel from direct coal liquefaction. Fuel 2014. doi:10.1016/j.fuel.2013.12.032.

[10] Yin B, Yu S, Jia H, Yu J. Numerical research of diesel spray and atomization coupled cavitation by Large Eddy Simulation (LES) under high injection pressure. Int J Heat Fluid Flow 2016;59:1–9. doi:10.1016/j.ijheatfluidflow.2016.01.005.

[11] Suh HK, Lee CS. Effect of cavitation in nozzle orifice on the Diesel fuel atomization characteristics. Int J Heat Fluid Flow 2008;29:1001–9. doi:10.1016/j.ijheatfluidflow.2008.03.014.

[12] Payri R, Salvador FJ, Gimeno J, De la Morena J. Analysis of Diesel spray atomization by means of a near-nozzle field visualization technique. At Sprays 2011;21:753–74. doi:10.1615/AtomizSpr.2012004051.

[13] Dumouchel C. On the experimental investigation on primary atomization of liquid streams. Exp Fluids 2008;45:371–422. doi:10.1007/s00348-008-0526-0.

[14] Salvador FJ, Ruiz S, Gimeno J, De la Morena J. Estimation of a suitable Schmidt number range in diesel sprays at high injection pressure. Int J Therm Sci 2011;50:1790–8. doi:10.1016/j.ijthermalsci.2011.03.030.

[15] Kiplimo R, Tomita E, Kawahara N, Yokobe S. Effects of spray impingement , injection parameters , and EGR on the combustion and emission characteristics of a PCCI diesel engine. Appl Therm Eng 2012;37:165–75. doi:10.1016/j.applthermaleng.2011.11.011.

[16] Idicheria CA, Pickett LM. Soot formation in Diesel combustion under high-EGR conditions. SAE Tech Pap 2005-01-3834 2005. doi:10.4271/2005-01-3834.

[17] Khalek IA, Blanks MG, Merritt PM, Zielinska B. Regulated and unregulated

emissions from modern 2010 emissions-compliant heavy-duty on-highway diesel engines. J Air Waste Manage Assoc 2015;65:987–1001. doi:10.1080/10962247.2015.1051606.

[18] Bergstrand P, Denbratt I. Diesel combustion with reduced nozzle orifice diameter. SAE Tech Pap 2001-01-2010 2001. doi:10.4271/2001-01-2010.

[19] Aori G, Hung DLS, Zhang M. Effect of Nozzle Configuration on Macroscopic Spray Characteristics of Multi-Hole Fuel Injectors Under Superheated Conditions. At Sprays 2016;26:439–62. doi:10.1615/AtomizSpr.2015011990.

[20] Siebers DL. Liquid-Phase Fuel Penetration in Diesel Sprays. SAE Tech. Pap. 980809, 1998. doi:10.4271/980809.

[21] Wan Y, Peters N. Scaling of spray penetration with evaporation. At Sprays 1999;9:111–32.

[22] Martínez-Martínez S, Sánchez-Cruz FA, Riesco-Ávila JM, Gallegos-Muñoz A, Aceves SM. Liquid penetration length in direct diesel fuel injection. Appl Therm Eng 2008;28:1756–62. doi:10.1016/j.applthermaleng.2007.11.006.

[23] Zama Y, Odawara Y, Furuhata T. Experimental Study on Velocity Distribution of Postimpingement Diesel Spray on a Wall. Part 2: Effect of ambient gas density and injection pressure on flow pattern. At Sprays 2016;26:921–38.

[24] Andreassi L, Ubertini S, Allocca L. Experimental and numerical analysis of high pressure diesel spray-wall interaction. Int J Multiph Flow 2007;33:742–65. doi:10.1016/j.ijmultiphaseflow.2007.01.003.

[25] Argueyrolles B, Dehoux S, Gastaldi P, Grosjean L, Levy F, Michel A, et al. Influence of injector nozzle design and cavitation on coking phenomenon. SAE Tech Pap 2007-01-1896 2007. doi:10.4271/2007-01-1896.

[26] Payri R, Salvador FJ, Gimeno J, Garcia A. Flow regime effects over non-cavitating Diesel injection nozzles. J Automob Eng 2011;226:133–44.

[27] Yu B, Fu PF, Zhang T, Zhou HC. The influence of back pressure on the flow discharge coefficients of plain orifice nozzle. Int J Heat Fluid Flow 2013;44:509–14. doi:10.1016/j.ijheatfluidflow.2013.08.005.

[28] Sun Z-Y, Li G-X, Chen C, Yu Y-S, Gao G-X. Numerical investigation on effects of nozzle's geometric parameters on the flow and the cavitation characteristics within injector's nozzle for a high-pressure common-rail DI diesel engine. Energy Convers Manag 2015;89:843–61. doi:10.1016/j.enconman.2014.10.047.

[29] Som S, Ramírez AI, Longman DE, Aggarwal SK. Effect of nozzle orifice geometry on spray, combustion, and emission characteristics under diesel engine conditions. Fuel 2011;90:1267–76. doi:10.1016/j.fuel.2010.10.048.

[30] Brusiani F, Falfari S, Pelloni P. Influence of the diesel injector hole geometry on the flow conditions emerging from the nozzle. Energy Procedia 2014;45:749–58. doi:10.1016/j.egypro.2014.01.080.

[31] He Z, Guo G, Tao X, Zhong W, Leng X, Wang Q. Study of the effect of nozzle hole shape on internal flow and spray characteristics. Int Commun Heat Mass Transf 2016;71:1–8. doi:10.1016/j.icheatmasstransfer.2015.12.002.

[32] Payri R, Salvador FJ, Gimeno J, De la Morena J. Study of cavitation phenomena

based on a technique for visualizing bubbles in a liquid pressurized chamber. Int J Heat Fluid Flow 2009;30:768–77. doi:10.1016/j.ijheatfluidflow.2009.03.011.

[33] Mitroglou N, Gavaises M. Mapping of cavitating flow regimes in injectors for medium-/heavy-duty diesel engines. Int J Engine Res 2013;14:590–605. doi:10.1177/1468087413500491.

[34] Salvador FJ, Hoyas S, Novella R, Martínez-López J. Numerical simulation and extended validation of two-phase compressible flow in diesel injector nozzles. Proc Inst Mech Eng Part D J Automob Eng 2011;225:545–63. doi:10.1177/09544070JAUTO1569.

[35] Payri F, Payri R, Salvador FJ, Martínez-López J. A contribution to the understanding of cavitation effects in Diesel injector nozzles through a combined experimental and computational investigation. Comput Fluids 2012;58:88–101. doi:10.1016/j.compfluid.2012.01.005.

[36] Salvador FJ, Martínez-López J, Romero J V., Roselló MD. Computational study of the cavitation phenomenon and its interaction with the turbulence developed in diesel injector nozzles by Large Eddy Simulation (LES). Math Comput Model 2013;57:1656–62. doi:10.1016/j.mcm.2011.10.050.

[37] Qiu T, Song X, Lei Y, Dai H, Cao C, Xu H, et al. Effect of back pressure on nozzle inner flow in fuel injector. Fuel 2016;173:79–89. doi:10.1016/j.fuel.2016.01.044.

[38] Sou A, Hosokawa S, Tomiyama A, Akio T. Effects of cavitation in a nozzle on liquid jet atomization. Int J Heat Mass Transf 2007;50:3575–82.

doi:10.1016/j.ijheatmasstransfer.2006.12.033.

[39] Andriotis A, Gavaises M. Influence of vortex flow and cavitation on near-nozzle diesel spray dispersion angle. At Sprays 2009;19:247–61.

[40] Desantes JM, Payri R, Salvador FJ, De la Morena J. Influence of cavitation phenomenon on primary break-up and spray behavior at stationary conditions. Fuel 2010;89:3033–41. doi:10.1016/j.fuel.2010.06.004.

[41] Abderrezzak B, Huang Y. A contribution to the understanding of cavitation effects on droplet formation through a quantitative observation on breakup of liquid jet. Int J Hydrogen Energy 2016;41:15821–8. doi:10.1016/j.ijhydene.2016.04.209.

[42] Molina S, Salvador FJ, Carreres M, Jaramillo D. A computational investigation on the influence of the use of elliptical orifices on the inner nozzle flow and cavitation development in diesel injector nozzles. Energy Convers Manag 2014;79:114–27. doi:10.1016/j.enconman.2013.12.015.

[43] Salvador FJ, Carreres M, Jaramillo D, Martínez-López J. Comparison of microsac and VCO diesel injector nozzles in terms of internal nozzle flow characteristics. Energy Convers Manag 2015;103:284–99. doi:10.1016/j.enconman.2015.05.062.

[44] Bermúdez V, Payri R, Salvador FJ, Plazas AH. Study of the influence of nozzle seat type on injection rate and spray behavior. ImechE J Automob Eng 2005;219:677–89. doi:10.1243/095440705X28303.

[45] Fang T, Coverdill RE, Lee CF, White RA. Effects of injection angles on

combustion processes using multiple injection strategies in an HSDI diesel engine. Fuel 2008;87:3232–9. doi:10.1016/j.proci.2008.07.031.

[46] De la Morena J, Vassallo A, Peterson RC, Gopalakrishnan V, Gao J. Influence of Swirl Ratio on Combustion System Performance of a 0.4L Single-Cylinder Diesel Engine. THIESEL 2014 Conf. Thermo- Fluid Dyn. Process. Direct Inject. Engines, 2014, p. 1–19.

[47] Kim MY, Lee CS. Effect of a narrow fuel spray angle and a dual injection configuration on the improvement of exhaust emissions in a HCCI diesel engine. Fuel 2007;86:2871–80. doi:10.1016/j.fuel.2007.03.016.

[48] Salvador FJ, Carreres M, Jaramillo D, Martínez-López J. Analysis of the combined effect of hydrogrinding process and inclination angle on hydraulic performance of diesel injection nozzles. Energy Convers Manag 2015;105:1352–65. doi:10.1016/j.enconman.2015.08.035.

[49] De la Morena J, Neroorkar K, Plazas AH, Peterson RC, Schmidt DP. Numerical analysis of the influence of diesel nozzle design on internal flow characteristics for 2-valve diesel engine application. At Sprays 2013;23:97–118. doi:10.1615/AtomizSpr.2013006361.

[50] He Z, Tao X, Zhong W, Leng X, Wang Q, Zhao P. Experimental and numerical study of cavitation inception phenomenon in diesel injector nozzles. Int Commun Heat Mass Transf 2015;65:117–24. doi:10.1016/j.icheatmasstransfer.2015.04.009.

[51] Salvador FJ, De la Morena J, Martínez-López J, Jaramillo D. Assessment of

compressibility effects on internal nozzle flow in diesel injectors at very high injection pressures. Energy Convers Manag 2017;132:221–30. doi:10.1016/j.enconman.2016.11.032.

[52] Bosch W. The Fuel Rate Indicator: a New Measuring Instrument for Display of the Characteristics of Individual Injection. SAE Pap 660749 1966.

[53] Payri R, Salvador FJ, Gimeno J, Bracho G. A new methodology for correcting the signal cumulative phenomenon on injection rate measurements. Exp Tech 2008;32:46–9. doi:10.1111/j.1747-1567.2007.00188.x.

[54] Lichtarowicz AK, Duggins RK, Markland E. Discharge coefficients for incompressible non-cavitating flow through long orifices. J Mech Eng Sci 1965;7:210–9. doi:10.1243/JMES_JOUR_1965_007_029_02.

[55] Desantes JM, Lopez JJ, Carreres M, López-Pintor D. Characterization and prediction of the discharge coefficient of non-cavitating diesel injection nozzles. Fuel 2016;184:371–81. doi:10.1016/j.fuel.2016.07.026.